Electronic Supplementary Material (ESI) for Physical Chemistry Chemical Physics.

Manipulating the metal-to-insulator transitions of VO_2 by combining compositing and doping strategies

Xuanchi Zhou [a†], Haifan Li [a†], Yanlong Shang [a], Fanqi Meng [b], Ziang Li [a], Kangkang Meng [a], Yong Wu [a], Xiaoguang Xu [a], Yong Jiang [a], Nuofu Chen [c]*, and Jikun Chen [a]**

[a] *School of Materials Science and Engineering, University of Science and Technology Beijing, Beijing, 100083, China*

[b] *School of Materials Science and Engineering, Tsinghua University, Beijing 100084, China*

[c] *School of Renewable Energy, North China Electric Power University, Beijing 102206, China*

*Authors to whom correspondence should be addressed: jikunchen@ustb.edu.cn *(J. Chen),* nfchen@ncepu.edu.cn *(N. Chen) and* yjiang@ustb.edu.cn *(Y. Jiang).*

[†]*X. Zhou and H. Li contributed equally to this work.*

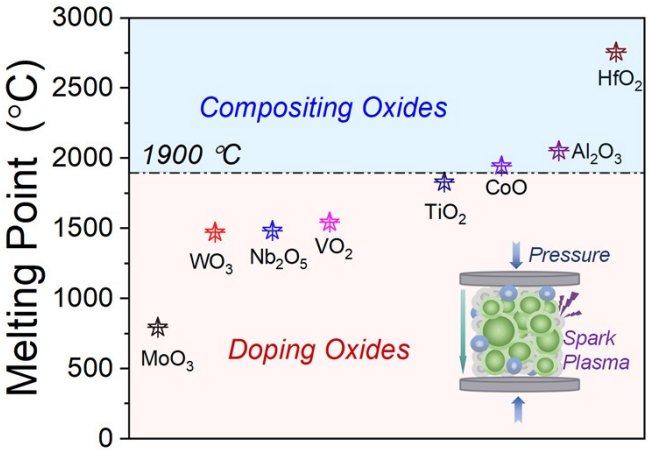

Figure S1. The melting points of as-used precursors oxides during the spark plasma assisted reactive sintering (SPARS) process. Substituting vanadium with doping elements can be achieved via introducing the low melting-point precursor oxides (e.g., below 1900 °C) as the dopants. In contrast, the high melting-point oxides (e.g., HfO_2, CoO and Al_2O_3) cannot be effectively diffused into the lattice of matrix VO_2 within the SPARS process.

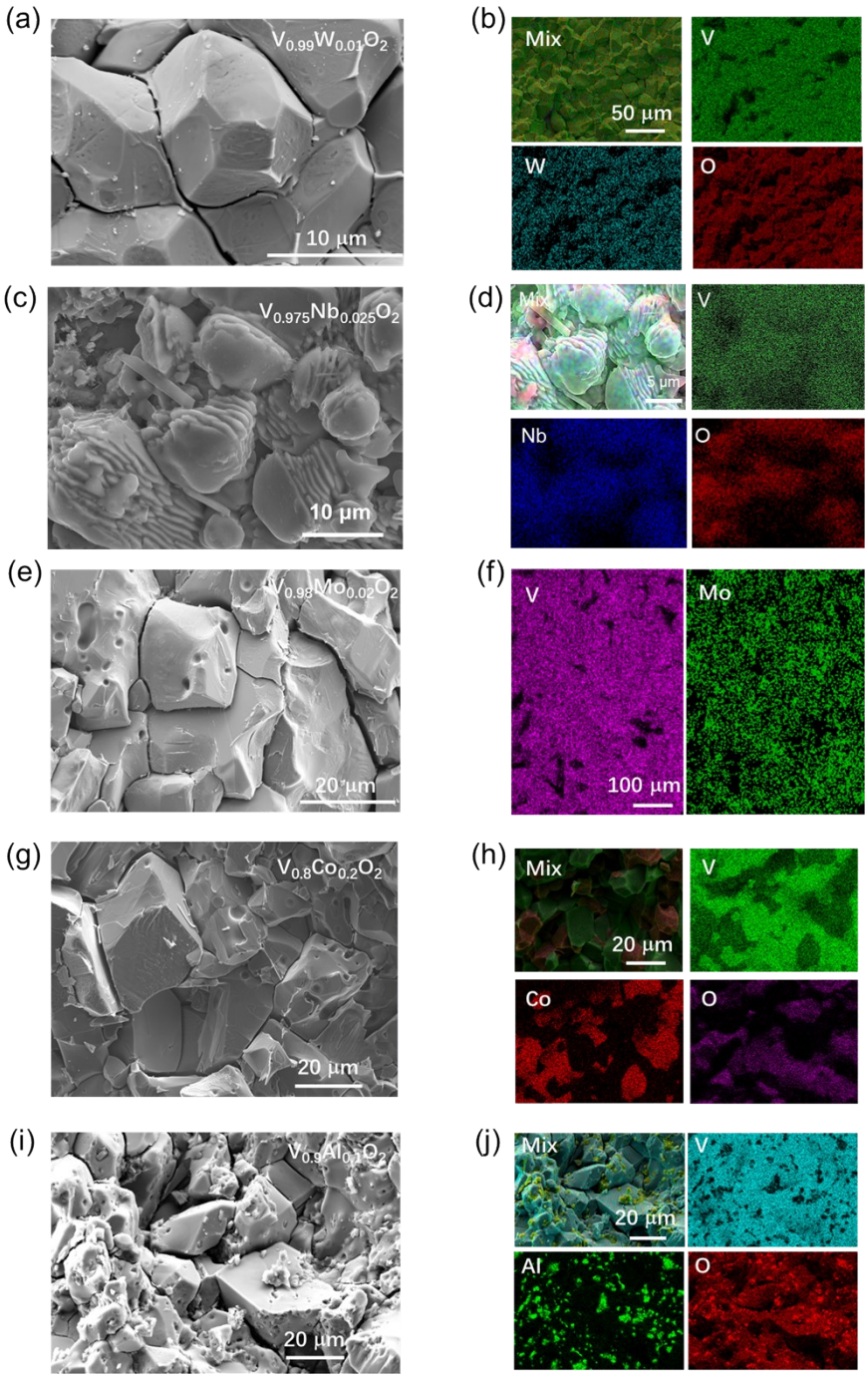

Figure S2. The cross-sectional surface morphologies from scanning electron microscopy (SEM) and respective elementary distributions as measured by energy dispersion spectrum (EDS) for composited VO_2 ceramic pellets. It can be seen that the as-sintered composited VO_2 ceramic pellets exhibit the polycrystallinity with a grain size of ~20 μm. In addition, the elementary distribution of compositing element is not observed for the region associated to the VO_2, and this indicates the less effective diffusion of high melting-point precursors oxides within VO_2 during the speak plasma assisted sintering process.

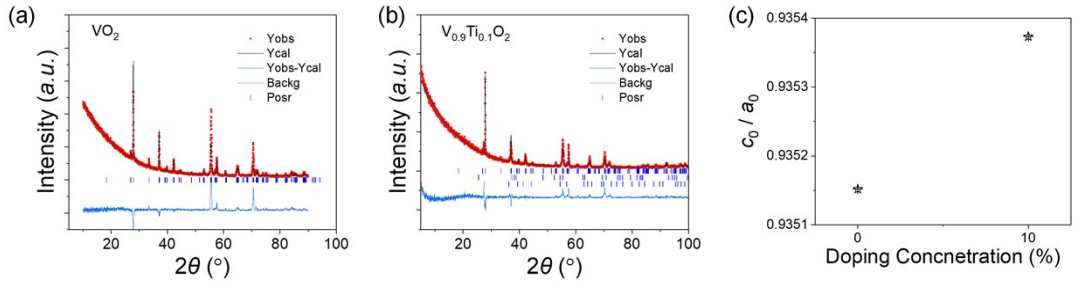

Figure S3. The Rietveld refinement of the X-ray diffraction (XRD) patterns of as-made (a) pristine VO_2, (b) $V_{0.9}Ti_{0.1}O_2$ ceramic pellets. (c) The ratio of the lattice constants (e.g., c_0/a_0) for Ti-doped VO_2 pellets plotted as a function of doping concentration. It can be seen that the enlarged magnitude of c_0/a_0 observed for $V_{0.9}Ti_{0.1}O_2$ sample indicates the local structural distortion upon Ti substitution, similar to the previous report [1].

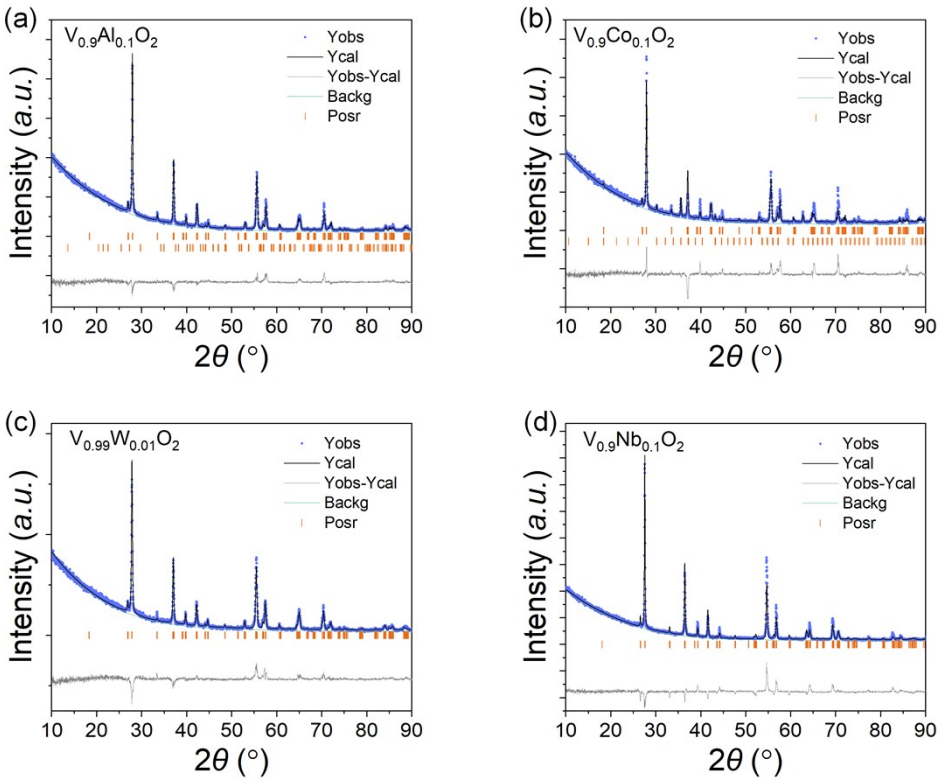

Figure S4. The Rietveld refinement of the X-ray diffraction (XRD) patterns of as-made (a) $V_{0.9}Al_{0.1}O_2$, (b) $V_{0.9}Co_{0.1}O_2$, (c) $V_{0.99}W_{0.01}O_2$ and (d) $V_{0.9}Nb_{0.1}O_2$ ceramic pellets. In general, the doped VO_2 ceramic pellets exhibit the same crystal structure to matrix VO_2 (M), while in contrast the peaks associated to precursor oxides with high melting point are clearly observed for composited VO_2 samples.

Table S1 Actual elementary concentration of as-made doped or composited VO_2 pellets.

Sample	Nominal concentration of vanadium (%)	Nominal concentration of doping elements (%)	Actual concentration of vanadium (%)	Actual concentration of doping elements (%)
$V_{0.99}W_{0.01}O_2$	99	1	99.09	0.91
$V_{0.995}W_{0.005}O_2$	99.5	0.5	99.56	0.44
$V_{0.9}Ti_{0.1}O_2$	90	10	89.86	10.14
$V_{0.8}Hf_{0.2}O_2$	80	20	80.22	19.78

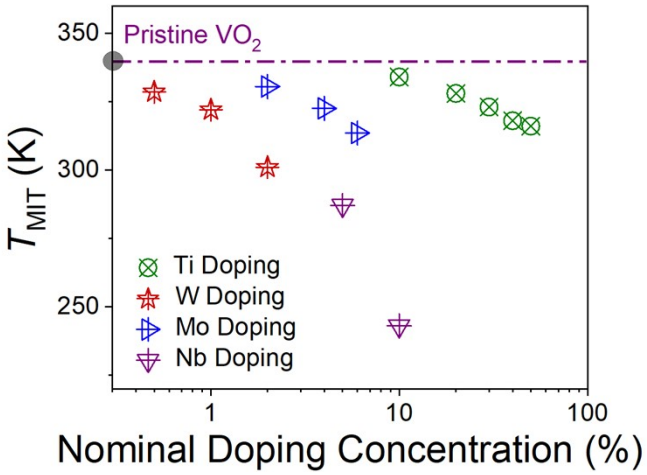

Figure S5. The transition temperature (e.g., T_{MIT}) of as-made doped VO_2 pellets (e.g., W^{6+}, Mo^{6+}, Nb^{5+} and Ti^{4+}) plotted as a function of the nominal doping concentration. It can be seen that the T_{MIT} for as-made doped VO_2 pellets (e.g., W^{6+}, Mo^{6+}, Nb^{5+} and Ti^{4+}) almost linearly reduces with an increasing doping concentration.

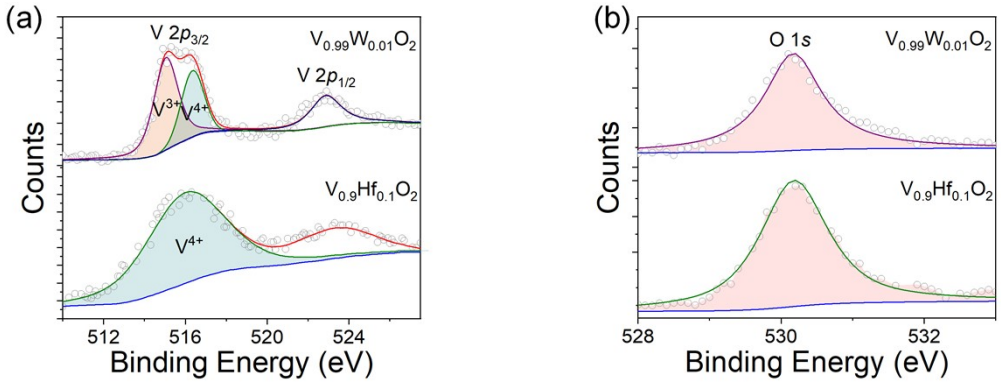

Figure S6. X-ray photoemission spectroscopy (XPS) analysis of (a) V and (b) O peaks as compared for $V_{0.99}W_{0.01}O_2$ and $V_{0.9}Hf_{0.1}O_2$ ceramic pellets. It can be seen that the valence state of vanadium is observed to be reduced towards +3 via W substitution, while the vanadium valence state of $V_{0.9}Hf_{0.1}O_2$ remains the same as +4. In addition, the main presence of lattice oxygen is observed for the O 1*s* peak of as-made $V_{0.99}W_{0.01}O_2$ and $V_{0.9}Hf_{0.1}O_2$ pellets. It is worthy to note that as-observed variations in the valence state of vanadium is in general consistency with the observations for their MIT functionalities.

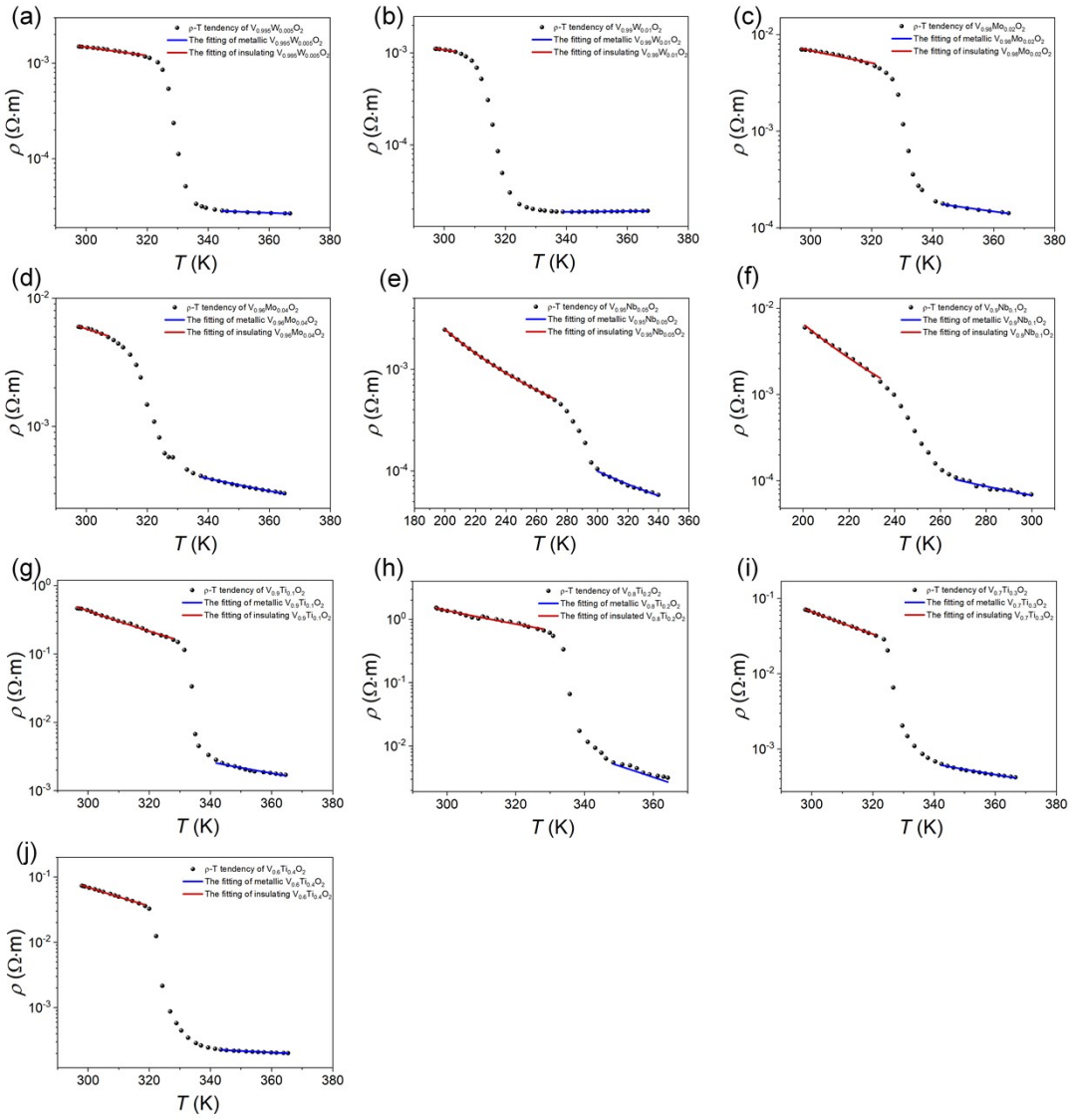

Figure S7. Fitting both the insulating and metallic phases for as-made doped VO_2 ceramic pellets (e.g., W^{6+}, Nb^{5+}, Mo^{6+} and Ti^{4+} doped) via the carrier hopping and two-phase models, respectively.

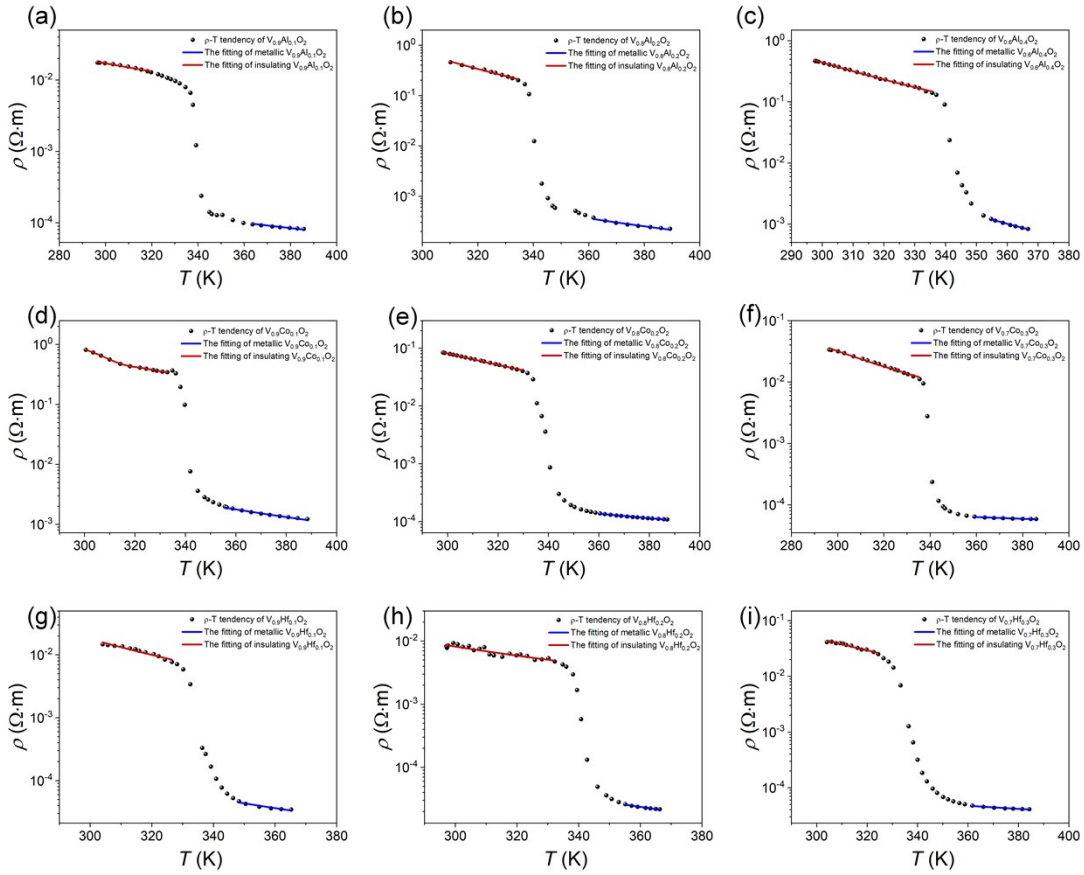

Figure S8. Fitting both the insulating and metallic phases for as-made composited VO_2 ceramic pellets (e.g., HfO_2, CoO and Al_2O_3 composited) via the carrier hopping and two-phase models, respectively.

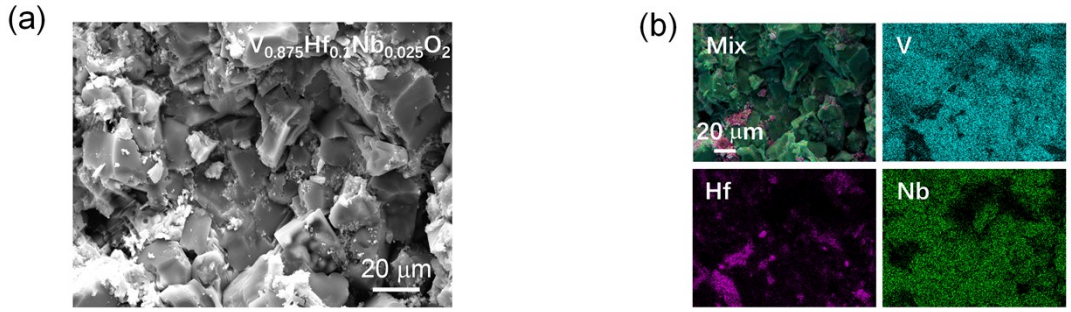

Figure S9. The cross-sectional surface morphology from scanning electron microscopy (SEM) and respective elementary distributions as measured by energy dispersion spectrum (EDS) mapping for co-doped VO_2 ceramic pellets. It can be seen that the same distribution is observed for substituted Nb and V elements, while the composited Hf element is not observed for the region of V element, indicating a successful fabrication of the co-doped ceramic pellet.

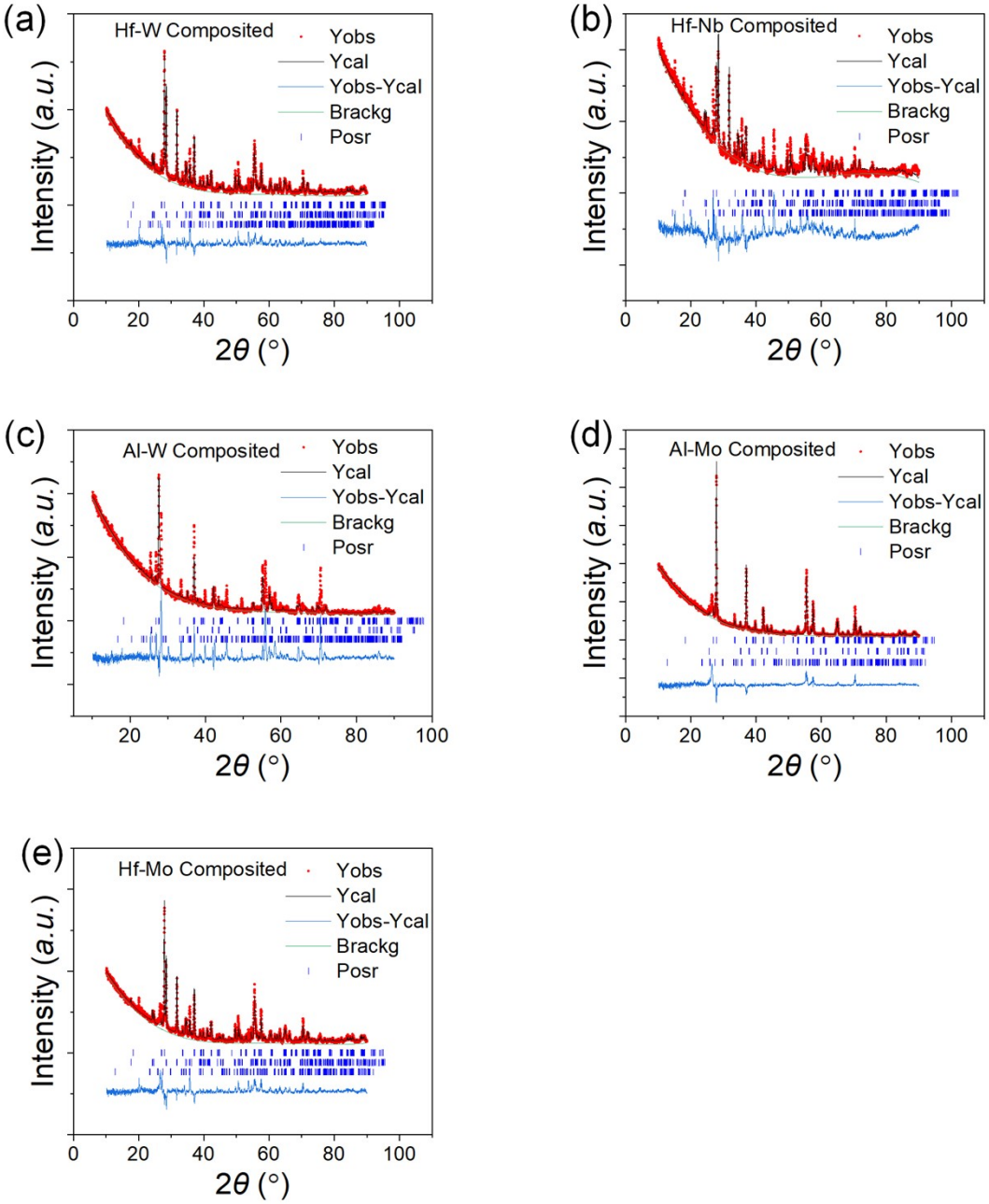

Figure S10. The Rietveld refinement of the X-ray diffraction (XRD) patterns of co-doped ceramic pellets.

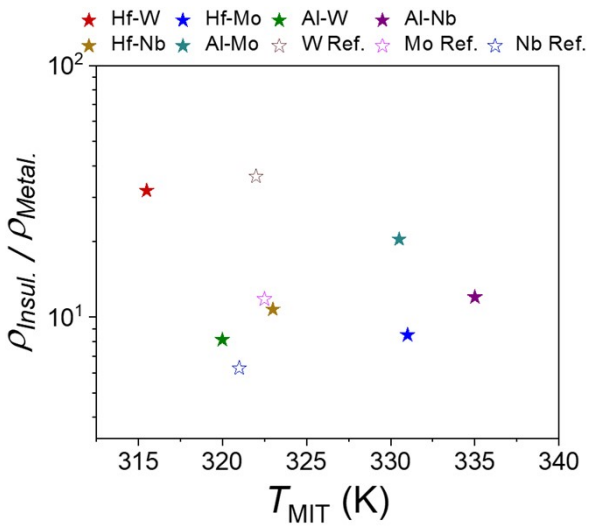

Figure S11. Transition sharpness (e.g., $\rho_{\text{Insul.}}/\rho_{\text{Metal.}}$) plotted as a function of the transition temperature (T_{MIT}) for as-made composited or doped VO_2, as compared with the previously reported one [2]. It can be seen that the T_{MIT} of co-doped ceramic pellet is reduced towards low temperature, owing to electron doping, while their respective transition sharpness is comparable to the ones for high-valence doped VO_2.

References

[1] C.N.R. Rao, M. Natarajan, G.V. Subba Rao, R.E. Loehman, Phase transitions and conductivity anomalies in solid solutions of VO_2 with TiO_2, NbO_2, and MoO_2, J. Phys. Chem. Solids. 32 (1971) 1147-1150.

[2] X. Zhou, Y. Cui, Y. Shang, H. Li, J. Wang, Y. Meng, X. Xu, Y. Jiang, N. Chen, J. Chen, Non-equilibrium Spark Plasma Reactive Doping Enables Highly Adjustable Metal-to-Insulator Transitions and Improved Mechanical Stability for VO_2, J. Phys. Chem. C. 127 (2023) 2639-2647.